



Effect of plasma treatment of copper on its corrosion behaviour in 3.5 % NaCl solution



O.A. González Noriega^a, J. Porcayo-Calderon^b, H. Martinez^c, R. Lopez-Sesenes^d,
J.G. Gonzalez-Rodriguez^{e,*}

^a Universidad Autónoma Nacional de México, Facultad de Química, Circuito Universitario, D.F. México, Mexico

^b Departamento de Ingeniería Química y Metalurgia, Universidad de Sonora, Hermosillo 83000, Mexico

^c Universidad Nacional Autónoma de México, Instituto de Ciencias Físicas, Av. Universidad S/N, Col. Chamilpa, 62209 Cuernavaca, Mor, Mexico

^d Universidad Autónoma del Estado de Morelos, FCQel, Av. Universidad 1001, Col. Chamilpa, 62209 Cuernavaca, Mor, Mexico

^e Universidad Autónoma del Estado de Morelos, CIICAp, Av. Universidad 1001, Col. Chamilpa, 62209 Cuernavaca, Mor, Mexico

ARTICLE INFO

Keywords:

Copper
Corrosion
Thermochemical treatment
Plasma oxidation

ABSTRACT

The influence of plasma preoxidation treatment on the corrosion behaviour of copper in a 3.5 % NaCl solution was evaluated. The electrochemical techniques used included potentiodynamic polarization curves, electrochemical impedance spectroscopy and linear polarization resistance at 20, 40 and 60 °C. The results showed that the preformed oxides included both cupric (CuO) and cuprous oxides (Cu₂O). Potentiodynamic polarization curves showed a reduction in the corrosion current density value by one order of magnitude in the plasma-oxidized specimens. However, for longer exposure times, the corrosion rates were higher for the plasma-oxidized specimens. Corrosion rates increased with an increase in the testing temperature. The corrosion mechanism was changed by the plasma treatment since it was under charge control for the as-received specimens, whereas a diffusion-controlled mechanism was active for the plasma-oxidized specimens at temperatures of at least 20 °C.

1. Introduction

The practical properties of copper make it one of the most widely used metallic materials in various fields. Its characteristics include high electrical and thermal conductivity, ease of joining, resistance to corrosion, high malleability, ductility, ease of combination with other metals, recyclability or secondary use, antimicrobial properties, non-magnetic properties, etc. [1–6]. Its applications range from water pipes, heat exchangers, electrical wiring, and printed circuit boards, among others [7–12]. However, despite having good resistance towards a uniform type of corrosion, pitting corrosion of copper and its alloys remains a concern in environments containing ammonia, CO₂-containing steam, sulfides, and chlorides [13–19]. Some methods used to improve the corrosion resistance of copper and its alloys include the use of coatings and inhibitors. [20–29]. To protect the environment, people have opted for the application of green inhibitors and coatings [2,3,6,14–16].

Thermochemical treatments are used to improve properties such as mechanical, tribological and corrosion resistance. Some such

treatments that we can mention are plasma nitriding and oxidation. Among its eminent advantages, such as the ability to treat parts with complex shapes, low treatment time and low temperature compared to traditional methods, plasma nitriding is also friendly to the environment [7,8,10,19,30–32]. For instance, Wei et al. [30] deposited Cr-based coatings on Zircalloy 4 by using the plasma method and evaluated their oxidation resistance in pressure water and boiling water reactor conditions at 360 °C. The weight gain for the coated alloy was 10 times lower than that for the uncoated alloy. Bayrak et al. [31] used both anodic and plasma oxidation of Ti6Al4V alloys to improve their wear and corrosion resistance in a human body simulated solution. Finally, Poplavsky used plasma to oxidize different metallic alloys, including carbon steel, stainless steels and pure aluminium, to protect them from the corrosion of sulfuric acid. As we know, some materials tend to form a passive layer after corrosion, which allows the material to protect itself and considerably slows the rate of corrosion [33]. By applying the plasma oxidation method, we are controlling the atmosphere in which the material is being corroded and accelerating a process that can take years; here, we do it in a few hours.

* Corresponding author.

E-mail address: ggonzalez@uaem.mx (J.G. Gonzalez-Rodriguez).

From a thermodynamic point of view, increasing seawater temperature usually accelerates electrochemical reactions in a metal when all other parameters are held constant. However, this condition cannot be achieved; therefore, the influence of temperature will be analysed based on the variation caused by the previously mentioned factors. For instance, an increase in seawater temperature increases both oxygen solubility and biological activity. By increasing the seawater temperature, the corrosion rate of copper increases several times; however, at temperatures above 60 °C, the corrosion rate decreases due to the dominating effect of reduced dissolved oxygen levels [11]. Thus, the purpose of the present research paper is to protect copper from corrosion through its passive layer [6,7,19] formed by the plasma oxidation method in 3.5 % NaCl solution at different testing temperatures.

2. Experimental procedure

2.1. Testing material

The material used in this work was 6.00 mm cylindrical bars of pure Cu, which was cut into 1.00 cm long samples. Samples were devasted with 2000 grade silicon carbide sandpaper. Afterwards, they were polished with 3.00 μ m alumina, washed with acetone and stored in a desiccator for later use.

2.2. Preoxidation treatment

The preoxidation of the samples was carried out under a 100 % oxygen atmosphere with the following working conditions: vacuum pressure of 1×10^{-3} torr, work pressure of 3.0 torr, current of 2.6×10^{-6} A, potential of 338 V and temperature of 550 °C. The distance between the electrodes was 4 mm.

2.3. Electrochemical tests

As a corrosive medium, a solution of NaCl at 3.5 % (wt%) was prepared using double distilled water. The volume of electrolyte used for the tests was 100 ml, and the testing temperatures were 20, 40 and 60 °C. The electrochemical techniques used were potentiodynamic polarization curves, open circuit potential (OCP), linear polarization resistance (LPR) and electrochemical impedance spectroscopy (EIS). For these tests, a three-electrode electrochemical cell was used, namely, a working electrode (samples with and without preoxidation treatment), a saturated calomel reference electrode (HgCl₂/Hg) and an auxiliary graphite electrode. Potentiodynamic polarization curves were made by polarizing the working electrode from -300 mV to 1000 mV with respect to its corrosion potential, E_{corr} , at a scan rate of 1 mV/s. Corrosion current density values, I_{corr} , were determined by using Tafel extrapolation. Open circuit potential measurements were made at hourly intervals throughout the test, which lasted 24 h. Linear polarization resistance measurements (LPR) were made by polarizing the working electrode ± 10 mV at a scan rate of 60 mV/min, and measurements were made at hourly intervals throughout the test, which lasted 24 h. Electrochemical impedance spectroscopy measurements (EIS) were performed by applying an alternating current (AC) signal with an amplitude of ± 10 mV in a frequency range from 100 kHz to 0.01 Hz. The formed oxides before and after corrosion tests were analysed in a Bruker Alpha Senterra II Raman Confocal Microscope, whereas morphological aspects were analysed in a low vacuum LEO Scanning Electronic microscope.

3. Results and discussion

3.1. Surface characterization of samples

The appearance of the Cu surface after plasma preoxidation treatment is shown in Fig. 1. From these micrographs, it is possible to

observe the formation of a continuous layer of copper oxide at low magnification (Fig. 1a); however, at higher magnification (Fig. 1b), the presence of surface irregularities such as porosity and filiform formation of the surface oxide can be seen, and a spongy appearance of the oxide is appreciated, which suggests the presence of microporosity.

Both as-received copper and plasma preoxidized copper were characterized by Raman spectroscopy, which can be seen in Fig. 2. In the case of the as-received specimen, without plasma oxidation treatment, we can slightly visualize a peak of the possible formation of cuprous oxide Cu₂O at a Raman shift value of 109 cm⁻¹, which could have been formed during transport or elemental analyses. When copper is in contact with oxygen, the first oxide to form is cuprous oxide, Cu₂O.

In the case of the plasma peroxidised specimen, we can clearly visualize the peaks of the oxides formed during the thermochemical process, giving rise to cuprous oxide, Cu₂O, at Raman shift values of 109, 150 and 520 cm⁻¹, whereas the presence of cupric oxide, CuO, is observed at the Raman shift value of 625 cm⁻¹. After analysing the comparative spectra in detail, we can visualize how the preoxidation treatment was successfully achieved by forming the respective oxides.

3.2. Open circuit potential (OCP)

Fig. 3 shows the evolution as a function of time of the open circuit potential value, OCP, for both as-received and plasma-oxidized copper specimens evaluated in a 3.5 % NaCl solution at different temperatures.

According to this figure, at 20 °C, the OCP values shifted rapidly towards nobler values during the first 3 h of immersion, and subsequently, a more or less steady state value was achieved until the end of the test; this trend may be due to the development and growth of a protective oxide on the surface of the copper. On the other hand, at 40 °C, the OCP values also show a great increase towards more positive values as time passes, up to 6 h of immersion, but for longer exposure times, the OCP values show a quasi-stationary behaviour, although they sifted towards more active values during the final part of the test. Similar to those observed at 20 and 40 °C, at 60 °C, a rapid increase in the OCP value was observed from the beginning of the test until 7 h of immersion, and subsequently, these values remained more or less constant, but in the final hours of testing, they went towards more active values, which, similar to at 40 °C, suggests that the developed oxide began to be dissolved.

It is interesting to note that all the curves show a similar slope at the beginning of the test, which suggests that the initial rate of formation of the protective oxide is similar. However, both the time required to reach the maximum point and the subsequent behaviour indicate different protective characteristics of the oxides developed. On the one hand, at 20 °C, the shortest time was observed to reach the first maximum, and subsequently, the OCP values increased constantly, which suggests the rapid formation of a protective oxide and a subsequent increase in its protective capacity. On the other hand, at 40 °C, the time required to reach the maximum was longer than that observed at 20 °C, and the subsequent behaviour suggests the formation of an oxide with surface defects that allowed the diffusion of the electrolyte towards the substrate. Finally, at 60 °C, the time required to reach the first maximum was much longer than that observed at 20 °C, and the subsequent behaviour suggests the development of an oxide that did not present protective characteristics, possibly due to the presence of a greater quantity of surface defects. Despite the fact that the noblest OCP values were obtained at 60 °C, the protective capacity of the developed oxide depends on the integrity of the layer formed (porosity, cracks) [20].

The evolution as a function of time of the OCP values of preoxidized copper evaluated in a 3.5 % NaCl solution at different temperatures is given in Fig. 4. At 20 °C, an abrupt shift in the OCP values in the active direction is observed in the first hour of immersion, and then they reach a steady state value until the end of the test. This behaviour may be due to dissolution of any formed protective oxide [34]. However, at 40 °C, the opposite effect was observed, namely, a shift towards nobler values

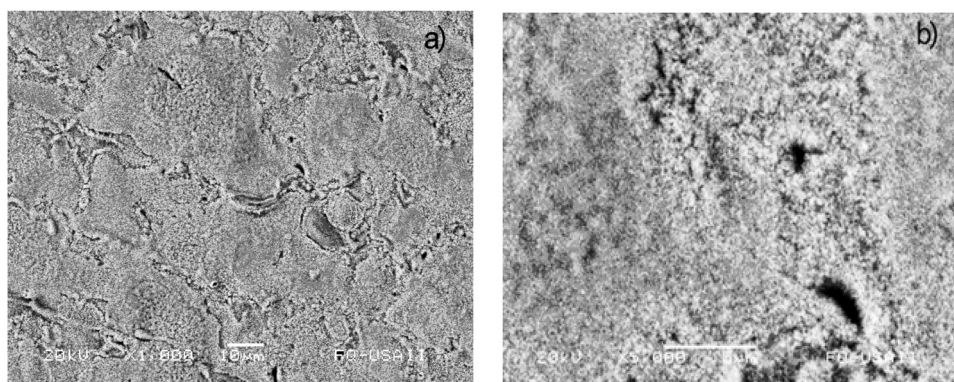


Fig. 1. Morphological aspects of the Cu surface after plasma treatment.

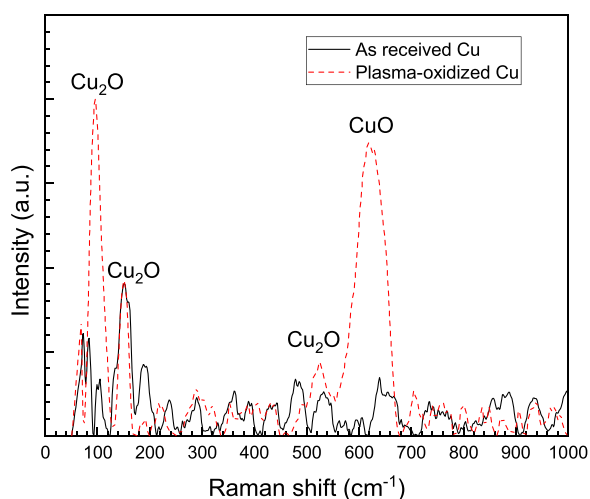


Fig. 2. Raman spectra of the as-received and plasma-oxidized specimens.

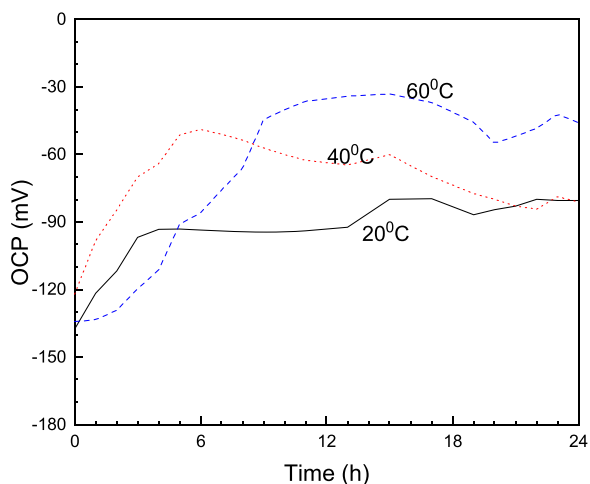


Fig. 3. Open circuit potential as a function of time for the as-received copper evaluated in a 3.5 % NaCl solution at different temperatures.

from the beginning of the test until 4 h of immersion, and after that, a slight increase and a quasistable behaviour in the last hours of immersion. This suggests that the preformed protective oxide increased its protective capacity possibly due to its surface self-sealing or increased the thickness of the protective oxide. At 60 °C, a shift in OCP values towards slightly more active values was observed in the first hour of immersion, probably due to the dissolution of any preformed oxide, but subsequently, the values went into the noble direction until they reached a steady state value, a behaviour similar to that observed at

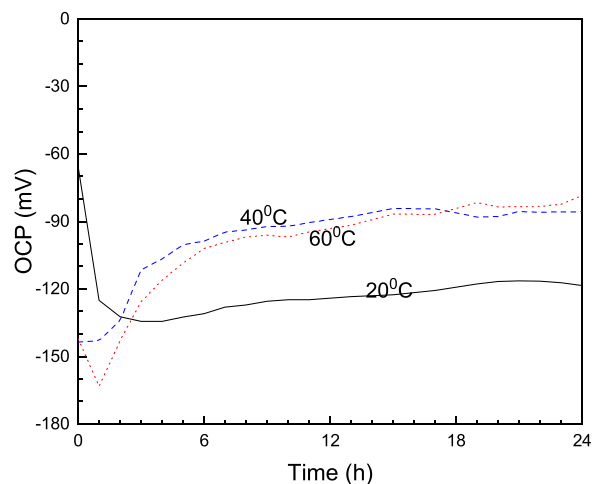


Fig. 4. Open circuit potential as a function of time for plasma preoxidized copper, evaluated in a 3.5 % NaCl solution at different temperatures.

40 °C [11,12]. The above behaviour suggests that the plasma treatment was not able to develop defect-free protective oxides. It is interesting to note that in the particular cases of the tests at 40 and 60 °C, their OCP values tend to the same value achieved by copper without plasma treatment at 20 and 60 °C at the end of the test (Fig. 3). It is possible that at 20 °C, the same values are reached at longer immersion times, which would be as expected since the protective layer formed or preformed is the same. Thus, although at the beginning of the tests the obtained OCP values were nobler for the plasma preoxidized specimen than for the as-received specimen, at least at 20 °C, as testing time elapsed, the OCP values became more active for the plasma oxidized specimen, indicating a higher corrosion susceptibility. At 40 and 60 °C, the obtained OCP values were always slightly more active for the plasma-oxidized specimens than for the as-received specimens.

3.3. Potentiodynamic polarization curves

Fig. 5 shows the potentiodynamic polarization curves of the as-received copper evaluated in a 3.5 % NaCl solution at different temperatures. Electrochemical parameters such as E_{corr} and I_{corr} are given in Table 1.

As reported in some other research works [35–37], the data displayed in Fig. 5 show only active behaviour, without evidence of the formation of a passive layer, and Tafel behaviour could be observed. It is observed that by increasing the temperature of the solution, the E_{corr} values shift towards more active values. On the other hand, at 20 °C, the cathodic branch shows an activation behaviour by charge transfer in the evaluated potential range [13], and at higher temperatures, a shorter cathodic branch by activation of charge transfer is observed,

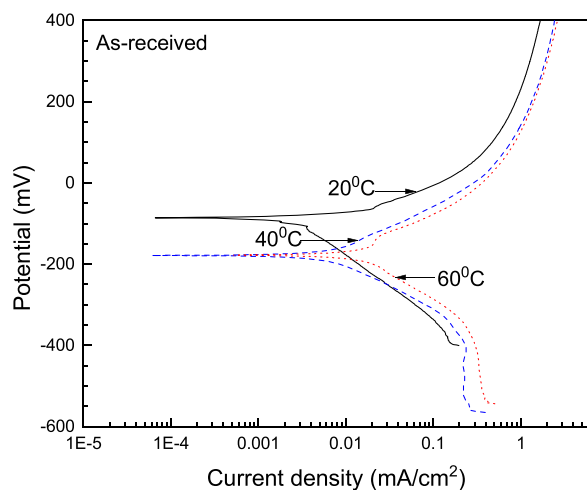


Fig. 5. Potentiodynamic polarization curve of copper in a 3.5 % NaCl solution at different temperatures.

and more negative potentials are detected in the presence of a limiting current due to mass transfer limitations. Table 1 shows that, in general, the I_{corr} value increases with increasing temperature by almost one order of magnitude. These values are in agreement with those reported previously [35–37].

On the other hand, for the plasma-oxidized specimens (Fig. 6), the polarization curves show that the corrosion potentials are approximately 120–150 mV. There were no noticeable shifts such as those shown by the as-received specimen. Similar to the as-received specimen, the polarization curves did not show evidence of the formation of a passive layer, only dissolution. At 20 °C, the anodic branch shows a change in its slope at potentials above 50 mV of its corrosion potential to exhibit a more active behaviour. This may be due to a loss of the protective ability of the preformed oxide. At higher temperatures, the observed anodic behaviour shows an active dissolution process. On the other hand, the cathodic branches exhibit very similar behaviour at all temperatures, and the absence of a limiting current, such as that observed in copper without treatment at 40 and 60 °C, is evident due to the mass transfer phenomenon. The I_{corr} values show a reduction in the corrosion rate of the preoxidized copper by approximately one order of magnitude at all testing temperatures. The effect of plasma preoxidation on the E_{corr} values depended on the temperature. In particular, at 20 °C, the E_{corr} value became more active for the plasma-oxidized specimen than that obtained without plasma treatment, whereas the opposite effect was observed at 40 and 60 °C.

3.4. Linear polarization resistance

The variation in the polarization resistance value, R_p , as a function of time for the as-received copper evaluated in a 3.5 % NaCl solution at different temperatures is shown in Fig. 7.

At 20 °C, copper shows a value close to 14,000 ohm cm^2 , which falls towards slightly lower values during the first hour of immersion, probably due to the dissolution of any protective oxide, and later on, this value shows a large increase until 12 h due to the formation of protective

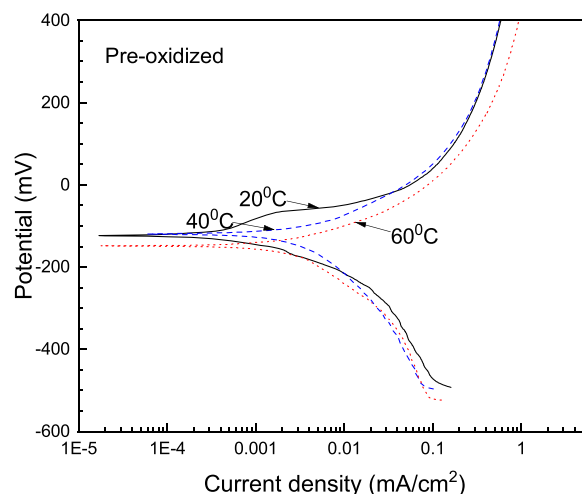


Fig. 6. Potentiodynamic polarization curves for copper with plasma pre-oxidation treatment in a 3.5 % NaCl solution at different temperatures.

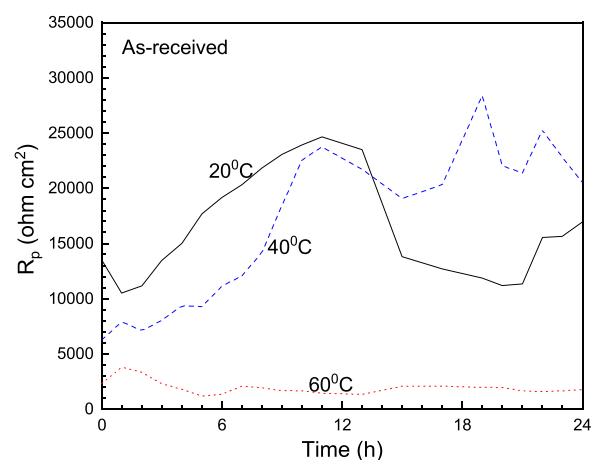


Fig. 7. Variation in the R_p value as a function of time for the as-received Cu evaluated in a 3.5 % NaCl solution at different temperatures.

corrosion products. At longer times, a decrease and an unstable trend are observed. At 40 °C, copper shows a constant increase in its R_p values up to 10 h of immersion, reaching values very similar to those observed at 20 °C. At 60 °C, although the R_p values were the lowest, the behaviour was more stable than those observed at 20 or 40 °C.

On the other hand, for the specimen with plasma preoxidation treatment, Fig. 8, the initial R_p value obtained at 20 °C was close to 20,000 ohm cm^2 , higher than that obtained for the as-received specimen, indicating a higher corrosion resistance given by the plasma-formed oxide in agreement with results obtained by the polarization curves; however, a rapid decrease in R_p values is observed followed by a quasi-stationary behaviour, which suggests a constant dissolution of the protective oxide and the presence of surface defects in the preformed oxide that allowed the copper-electrolyte contact and the subsequent self-sealing of the protective layer.

Table 1

Electrochemical parameters obtained from the polarization curves of Cu.

Specimen	E_{corr} (mV)			I_{corr} (mA/cm ²)		
	20°C	40°C	60°C	20°C	40°C	60°C
As-received	-86	-177	-179	0.0030	0.0101	0.028
Plasma-oxidized	-123	-119	-148	0.0004	0.0037	0.0052

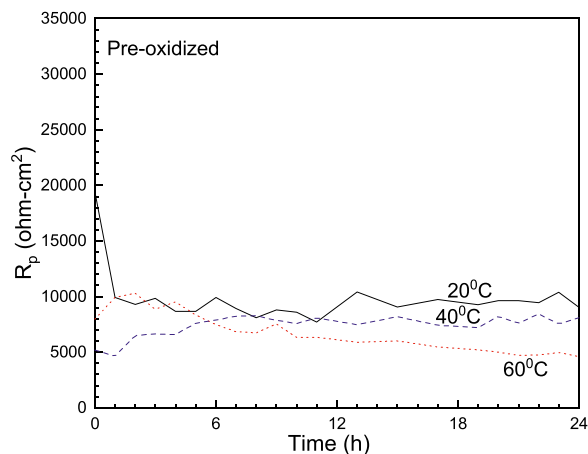


Fig. 8. Variation in the R_p value as a function of time for preoxidation evaluated in a 3.5 % NaCl solution at different temperatures.

At the beginning of the test, the R_p values obtained at 40 and 60 °C were lower than those attained at 20 °C; however, after a few hours of testing, the values obtained at the three different testing temperatures were virtually the same, with only small differences. Interestingly, the R_p values observed for the plasma-oxidized specimens were lower and fluctuated less than those obtained for the as-received specimen, which showed large fluctuations in their values. This may be due to the dissolution of the initially formed oxide for the plasma-treated specimen in the first hour of immersion and to an initial attempt to self-seal the surface defects of the preformed oxide. In addition, the plasma-formed oxide was more stable, with much fewer defects than the air-formed oxide in the as-received specimen.

3.5. Electrochemical impedance spectroscopy (EIS)

The effect of testing temperature on the Nyquist diagrams for both the as-received and plasma-oxidized copper evaluated in 3.5 % NaCl is shown in Fig. 9. For the as-received material, the Nyquist diagram for the tests at 20 °C displayed one depressed capacitive semicircle at high frequency values followed by a second capacitive loop at medium and lower frequency values. For the tests carried out at 40 and 60 °C, we can observe two very overlapping capacitive semicircles. The high-frequency semicircle is related to electrochemical reactions such as charge transfer carried out at the metal/double electrochemical layer interface, whereas the low-frequency loop is related to the electrochemical reaction carried out at the metal/corrosion product film interface [30–33].

As the testing temperature increases, the low-frequency semicircle diameter decreases as a result of the increase in the corrosion rate, decreasing from a value of nearly 22,000 ohm cm² for the test at 20 °C to a value of 13,000 ohm cm² for the test performed at 60 °C. On the other hand, the plasma-oxidized specimen has a different impedance response, since the Nyquist data for the test at 20 °C show the presence of a capacitive semicircle at high frequency values followed by what looks like a straight line at intermediate and lower frequencies, typical of a reactant diffusion-controlled corrosion process such as that reported in previous research [35–37]. At higher temperatures, however, the impedance response was similar to that observed in the as-received specimen, since a depressed capacitive semicircle is observed at high frequency values followed by a second capacitive loop at medium and lower frequency values. The diameter of the semicircle decreases with the testing temperature, which indicates a decrease in the corrosion rate. Compared to the tests carried out for the as-received specimen, a reduction in the semicircle diameter is observed for the plasma-oxidized specimens, which indicates an increase in the corrosion rate for the latter.

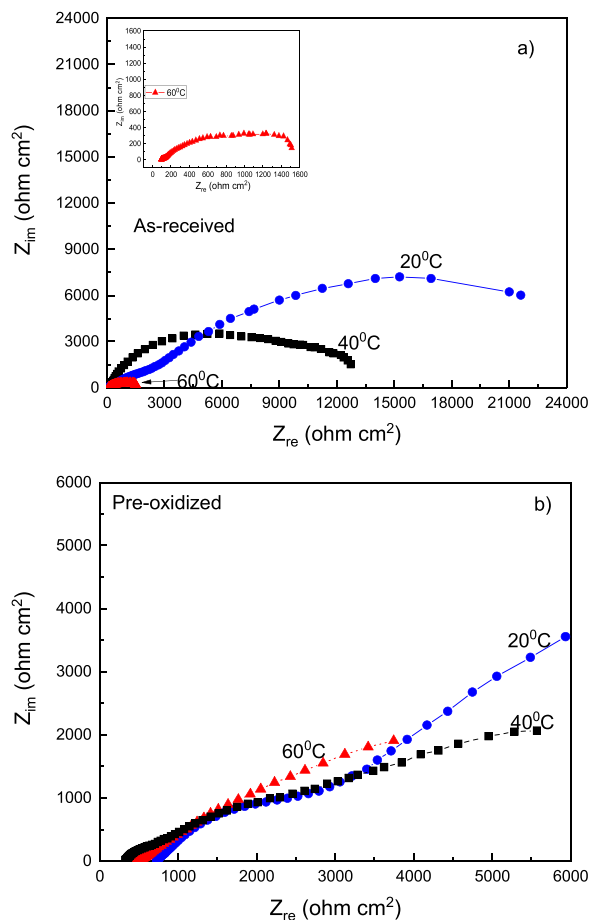


Fig. 9. Nyquist diagrams for the a) as-received and b) plasma-oxidized Cu evaluated in a 3.5 % NaCl solution at different temperatures.

Bode diagrams for both the as-received and plasma-oxidized copper specimens are given in Fig. 10. The interpretation of the Bode plots allows us to more precisely define the surface processes that occur on the working electrode. It has been suggested that their interpretation has to be based on frequency intervals: for the high frequency region (> 1000 Hz), the modulus is associated with the resistance of the electrolyte; the intermediate frequency region (10–1000 Hz) is associated with charge transfer processes, and the low frequency region (< 1–10 Hz) is associated with the surface processes mentioned above. Based on the above, from the Bode diagram in its impedance modulus format for the as-received specimen at 20 °C, Fig. 10, the apparent formation of the high-frequency plateau is observed at frequency values higher than 10,000 Hz, which suggests the absence of surface layers (metal hydroxide-type compounds). In the low- and intermediate-frequency regions, the presence of two linear relationships $\log f$ - $\log |Z|$ is visible, that is, the presence of two slopes and the absence of a low-frequency plateau. The magnitude of the impedance modulus in the low-frequency region is consistent with the variation in the diameter of the capacitive semicircles observed in the Nyquist diagram. The visible presence of two slopes suggests at least the existence of two time constants and therefore the presence of at least two capacitive semicircles in the Nyquist diagram.

For the case of the as-received specimen at 40 °C in the high frequency region, it is observed that the high frequency plateau is detected at frequencies greater than 1000 Hz, which suggests the formation and evolution of a time constant. This can be associated with the presence of surface films of the metal hydroxide or oxy-hydroxide type. At lower frequencies, the formation of two linear relationships $\log f$ - $\log |Z|$ is indicative of the presence of two time constants. The absence of a low-frequency plateau indicates that the value of the impedance module is

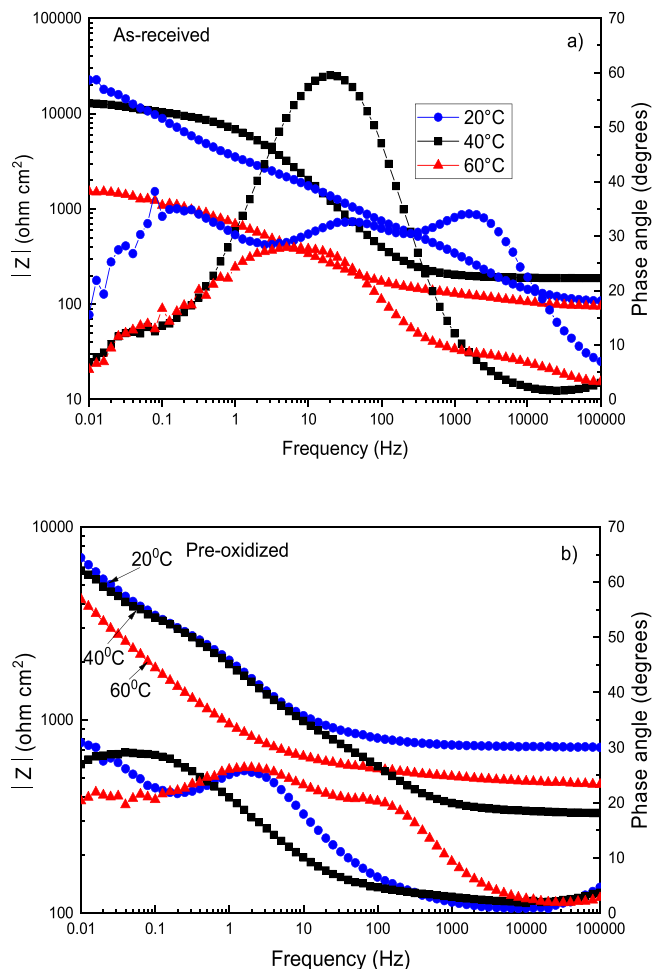


Fig. 10. Bode plots for the a) as-received and b) plasma-oxidized Cu evaluated in a 3.5 % NaCl solution at different temperatures.

greater than the last recorded value. The evolution of the values of the impedance module in the low-frequency region is in accordance with the evolution of the diameter of the capacitive semicircle observed in the Nyquist diagram.

In the case of the as-received specimen at 60 °C, it is observed that the high frequency plateau forms at frequencies higher than 1000 Hz. In the low- and intermediate-frequency regions, the presence of two linear relationships $\log f\text{-}\log |Z|$ suggests the formation of two time constants. Again, the presence of a high-frequency plateau is not observed, and the evolution of the impedance module in the low-frequency region is consistent with the evolution of the capacitive semicircle observed in the Nyquist diagram.

From the Bode plot, the phase angle format for the as-received specimen at 20 °C shows at least three peaks at 0.1, 30 and 2000 Hz with phase angle values of approximately 30 degrees, which indicates

the presence of at least 2 time constants. In the low-frequency region, the formation and evolution of a third time constant whose maximum phase angle remains fluctuating throughout the entire experimentation time is clearly observed. This time constant may be associated with species diffusion or adsorption processes as a consequence of the formation of the first time constant. For the test carried out at 40 and 60 °C, two peaks were displayed, at 0.05 and 10 Hz for the test at 40 °C and at 0.05 and 7 Hz for the test at 60 °C, indicating the presence of two time constants, whereas the phase angle values were 60 and 25 degrees, respectively. The displacement of the time constant at higher frequencies may be associated with an increase in the thickness of the protective oxide, and the decrease in its phase angle may be indicative of a decrease in the capacitive properties of the developed oxide.

On the other hand, for the plasma-oxidized specimens, in the Bode diagram in its impedance modulus format for the test at 20 °C in the high-frequency region, the formation of a high-frequency plateau is observed, which starts at approximately 10 Hz. Note the presence of two linear relationships $\log f\text{-}\log |Z|$. This suggests the presence of two time constants. In the low-frequency region, the formation of a corresponding plateau is not observed. For the test at 40 °C, a behaviour similar to that at 20 °C is observed; that is, in the high-frequency region, the formation of the corresponding plateau is visualized, and at lower frequencies, the presence of two relationships is observed: linear $\log f\text{-}\log |Z|$. Again, this suggests the presence of two time constants and the absence of a low-frequency plateau. In the case of the test at 60 °C, in the high frequency region, it is observed that the corresponding plateau is formed at frequencies greater than 100 Hz. In addition, the formation of three linear relationships $\log f\text{-}\log |Z|$ is observed, and the formation of a low-frequency plateau is not visible either.

From the Bode plot in its phase angle format for the material corroded at 20 °C in the high frequency region, it can be observed that the phase angle tends to 0 at frequencies greater than 100 Hz. At lower frequency values, the presence and evolution of two overlapping time constants are observed, the first between 1 and 10 Hz and the second at frequencies less than 0.02 Hz, whereas the highest phase angle value was 20 degrees. It is possible that the presence of the first time constant corresponds to the capacitive response of copper oxide formed by the plasma treatment, and the second time constant corresponds to the response to a diffusion process, possibly due to the presence of porosity in the preformed oxide.

This would justify the decrease in the maximum phase angle of the first time constant. For the material corroded at 40 °C, a behaviour similar to that at 20 °C is observed, that is, a phase angle that tends to 0 at frequencies greater than 100 Hz and the presence and evolution of two time constants, the first at approximately 50 Hz and the second at approximately 0.02 Hz. The meaning of these time constants is the same as those at 20 °C. The maximum phase angle value was also 20 degrees. In the case of the plasma preoxidized and corroded at 60 °C, the presence and evolution of three time constants is clear. The first time constant is located at approximately 100 Hz, the second at approximately 2 Hz and the third at frequencies less than 0.1 Hz. The characteristics of the first time constant suggest that its presence is due to the formation of a layer of surface corrosion products of the metal oxy-

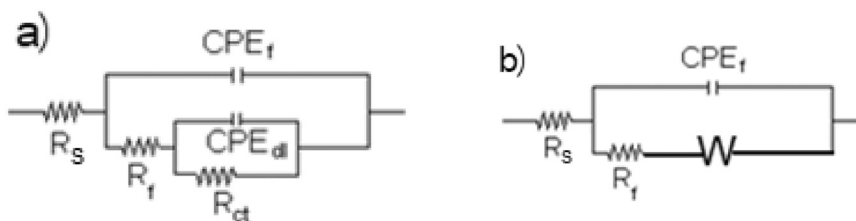


Fig. 11. Equivalent electric circuit used to simulate EIS data.

Table 2
Electrochemical parameters used to fit the EIS data for the as-received specimen.

T (°C)	R_s (ohm cm^2)	Y_{dl} (F/ cm^2)	n_{dl}	R_{dl} (ohm cm^2)	Y_f (F/ cm^2)	n_f	R_f (ohm cm^2)	$\gamma^2 \times 10^4$
20	205	3.4×10^{-5}	0.82	844	1.1×10^{-5}	0.91	21,045	2.9
40	92	7.9×10^{-5}	0.71	141	4.1×10^{-5}	0.82	13,540	8.4
60	85	4.9×10^{-4}	0.50	106	8.7×10^{-5}	0.73	1525	1.7

Table 3
Electrochemical parameters used to fit the EIS data for the plasma-oxidized specimen.

T (°C)	R_s (ohm cm^2)	Y_{dl} (F/ cm^2)	n_{dl}	R_{dl} (ohm cm^2)	Y_f (F/ cm^2)	n_f	R_f (ohm cm^2)	R_w (ohm cm^2)	$\gamma^2 \square 10^4$
20	730	1.2×10^{-4}	0.71	1636	–	–	–	5630	2.9
40	475	4.8×10^{-4}	0.62	1491	1.8×10^{-4}	0.72	5231	–	0.26
60	315	7.2×10^{-4}	0.42	1253	3.4×10^{-4}	0.51	4071	–	4.7

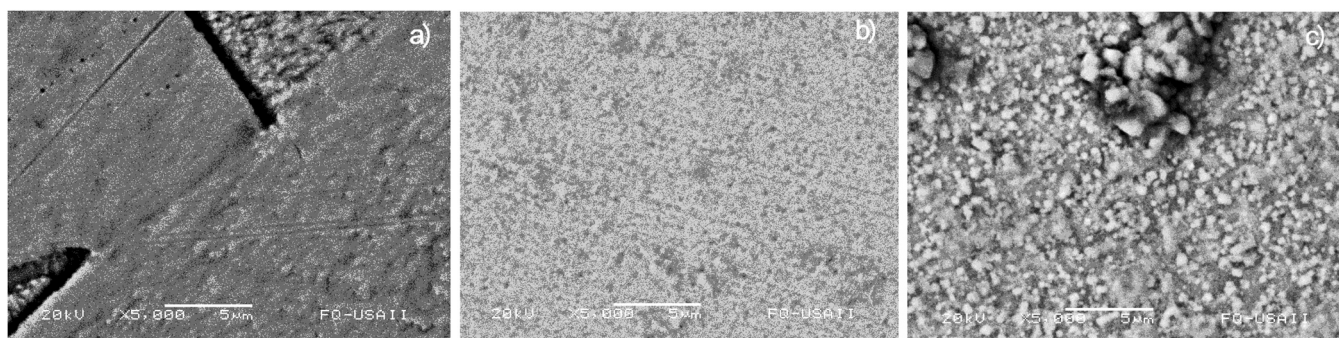


Fig. 12. Morphological aspects of the preoxidized Cu after the corrosion test in a 3.5 % NaCl solution at a) 20, b) 40 and c) 60 °C.

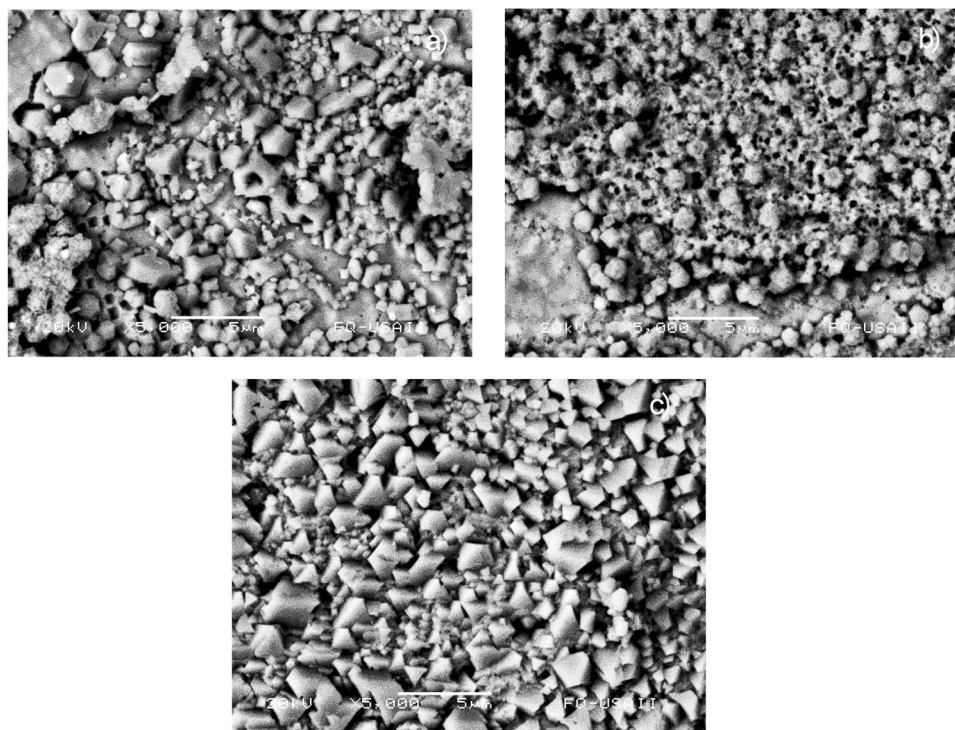


Fig. 13. Morphological aspects of the plasma-treated Cu surface after the corrosion test in a 3.5 % NaCl solution at a) 20, b) 40 and c) 60 °C.

hydroxide type, the second time constant corresponds to the capacitive response of the copper oxide preformed by the plasma treatment and the third time constant corresponds to the response to a diffusion process due to possibly to the presence of a surface layer of corrosion products. Interestingly, the phase angle values obtained in the plasma-oxidized specimens were much lower than those obtained in the as-

received specimens.

Based on what was discussed above, it is possible to establish the equivalent circuits shown in Fig. 11 for the modelling of the impedance spectra of Cu specimens corroded in the 3.5 % NaCl solution at the different test temperatures. In these circuits, the solution resistance is represented by R_s , whereas the charge transfer resistance is represented

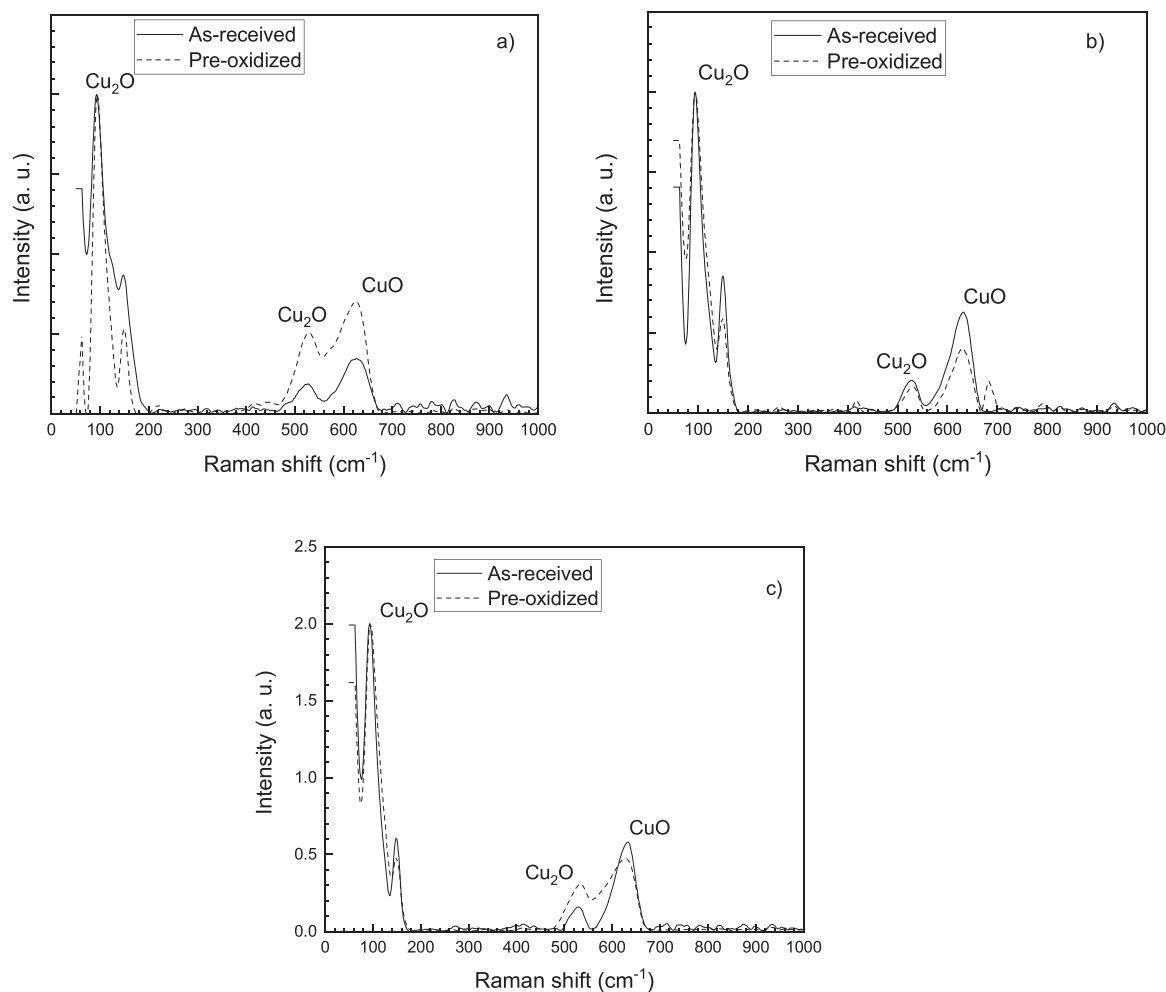


Fig. 14. Raman spectra of as-received and preoxidized copper samples after electrochemical tests in a 3.5 % NaCl solution at a) 20, b) 40 and c) 60 °C.

by R_{ct} , and the double electrochemical layer capacitance is represented by C_{dl} . In a similar way, the resistance of the film formed by the corrosion products is represented by R_f and its capacitance is represented by C_f . Finally, the Warburg impedance, which represents the reactant diffusion towards the metal surface, is represented by W , where the diffusion layer resistance is represented by R_w . In all cases, a constant phase element (CPE) was used instead of capacitance to compensate for surface irregularities such as roughness or irregular distribution of charge transfer and because the semicircles obtained are depressed. Its impedance value is a function of frequency, and the phase is independent of frequency:

$$Z_{CPE} = \frac{1}{Y(j\omega)^n} \quad (1)$$

where Y is the admittance of the system, a factor that combines properties related to the surface and electroactive species and is independent of the frequency; j is the imaginary unit ($\sqrt{-1}$); ω is the angular frequency ($\omega = 2\pi f$), where f is the frequency; and n is related to the slope of $\log|Z|$ vs. $\log|f|$. If n is equal to 1, the CPE is an ideal capacitor, where Y is equal to the capacitance; however, if $0.5 < n < 1$, then the CPE describes a distribution of dielectric relaxation times in the frequency space, and if $n = 0.5$, then the CPE represents the Warburg impedance. The calculated parameters obtained for fitting the EIS data for both the as-received and plasma-oxidized specimens are summarized in Tables 2 and 3, respectively.

In both cases, it can be seen that the R_f values are much higher than those for R_{ct} , indicating that the corrosion resistance is enhanced by the protective corrosion products formed on top of the specimens.

Additionally, these values were higher for the as-received specimen than for the plasma-oxidized specimen, explaining why the latter showed higher corrosion rates than the former. Both parameters decreased with increasing testing temperature, whereas the admittance increased, indicating an increase in the corrosion rate for both specimens. The R_{ct} values for the as-received copper specimen decreased with an increase in testing temperature, indicating that the corrosion process was under charge transfer control. On the other hand, for the plasma-oxidized specimen, the presence of the Warburg impedance for the test at 20 °C indicates a diffusion-controlled corrosion process, whereas at 40 and 60 °C, the process was under charge transfer control. When the n parameter value is close to 1, it indicates a low metal surface roughness due to a low dissolution rate, whereas a value close to 0.5 indicates a high metal surface roughness due to a high dissolution rate. Tables 2 and 3 indicate that the values for n decrease from values close to 1 down to 0.5 as the testing temperature increases, indicating an increase in the metal corrosion rate. Additionally, the n values for the as-received copper specimen are higher than those obtained for the plasma-oxidized specimen due to a higher corrosion rate for the latter than for the former.

3.6. Surface analysis of the corroded specimens

The appearance of the as-received Cu surface after the corrosion test at different testing temperatures is shown in Fig. 12. For the specimen corroded at 20 °C (Fig. 12a), the observed morphological aspects do not show evidence of severe damage caused by the electrolyte, and we observe a smooth surface. However, for the corroded specimen at 40 °C

(Fig. 12b), we observe a rougher surface than the corroded specimen at 20 °C, showing the presence of a compact layer of corrosion products, which is evidence that the specimen has undergone an attack by the electrolyte. For the specimen corroded at 60 °C (Fig. 12c), the formation of a continuous and homogeneous porous surface oxide is observed; however, it is possible to see the growth of small nodules on the entire surface. It is possible that the formation of these nodules is a consequence of localized attack due to the presence of defects developed in the first developed superficial layer [26–31].

On the other hand, plasma-oxidized specimens corroded at the different testing temperatures (Fig. 13) showed a large presence of corrosion products, perhaps oxides, which are very porous, allowing the penetration of the electrolyte in the form of crystals with a polyhedral structure. The formation of corrosion products in the form of octahedral crystals is appropriate for cuprite [26]. The appearance of the pre-oxidized Cu surface after the corrosion test at 40 °C is shown in Fig. 13b. From the micrographs, it is possible to observe a surface appearance similar to that observed at 20 °C. However, due to the increase in temperature, it is possible to observe a greater coverage of re-precipitated oxide formation, possibly due to an increase in the rate of metal dissolution [26]. The preoxidized Cu surface after the corrosion test at 60 °C (Fig. 13c) had corrosion products with qualitatively similar to those observed at 20 and 40 °C; however, the presence of a layer of oxide with a polyhedral structure adhered to the surface is notorious, and the remaining preformed oxide possibly re-precipitated. This type of morphology has been reported by other authors in some studies of copper, who established that cuprite crystallizes in a cubic system, whereas in favourable conditions for crystal growth, large octahedral crystals can be formed. When these large crystals adopt a random orientation, they result in a porous material that is permeable to small molecules and ions, facilitating the base metal corrosion process. This explains the relatively high corrosion rate for plasma-oxidized copper in seawater [12,26].

The Raman spectra of the samples after electrochemical tests in a solution of NaCl at 3.5 % are given in Fig. 14. It is clear from these spectra that all specimens exhibited on their corrosion product layer the formation of both cuprous oxide Cu₂O and cupric oxide CuO, which are responsible for the specimens' corrosion resistance, although, as evidenced by the SEM micrographs, the corrosion products formed in the plasma-oxidized specimens were much more porous than those formed in the as-received specimens. The formation of more porous oxides in the preoxidized specimens made the underlying metal less corrosion resistant, whereas the formation of compact oxides in the as-received specimens increased the substrate corrosion resistance.

4. Conclusions

A study of the plasma-oxidation process on the corrosion behaviour of Cu in a 3.5 % NaCl solution at different testing temperatures was carried out. The main findings can be summarized as follows:

1. The oxides formed by the plasma treatment included both CuO and Cu₂O, which were present in the as-received specimen.
2. Although at the beginning of the tests the OCP values were nobler for the plasma-oxidized specimen than those obtained for the as-received specimens, these values shifted towards more active values for the former.
3. Polarization curves did not show evidence of the formation of a passive layer either in the as-received specimens or in the plasma-oxidized ones. Nevertheless, I_{Corr} values were one order of magnitude lower for the latter.
4. The R_p values for all specimens decreased with increasing testing temperature; however, for the as-received specimens, they increased as time elapsed, whereas they decreased for the plasma-oxidized specimens.
5. The corrosion mechanism was under charge control for the as-

received specimens and for the plasma-oxidized specimen at 40 and 60 °C, whereas it was under diffusion control for the plasma-oxidized specimen tested at 20 °C.

Declaration of Competing Interest

The authors declare that they have no known competing financial interests or personal relationships that could have appeared to influence the work reported in this paper.

References

- [1] Z. Zaklina, Marija B. Tasic, Mihajlovic Petrovic, Milan B. Radovanovic, Milan M. Antonijevic, New trends in corrosion protection of copper, Chem. Pap. 73 (2019) 2103–2132, <https://doi.org/10.1007/s11696-019-00774-1>
- [2] N. Velazquez-Torres, H. Martínez, J. Porcayo-Calderon, E. Vazquez-Velez, J.G. Gonzalez-Rodriguez, L. Martinez-Gomez, Use of an amide-type corrosion inhibitor synthesized from the coffee bagasse oil on the corrosion of Cu in NaCl, Green Chem. Let. Rev. 11 (2017) 1–11, <https://doi.org/10.1080/17518253.2017.1404645>
- [3] K. Dahmani, M. Galai, M. Ouakki, M. Cherkaoui, R. Touri, S. Erkan, B.El Ibrahim, Quantum chemical and molecular dynamic simulation studies for the identification of the extracted cinnamon essential oil constituent responsible for copper corrosion inhibition in acidified 3.0 wt % NaCl medium, Inorg. Chem. Com. 124 (2021) 108409, <https://doi.org/10.1016/j.inoche.2020.108409>
- [4] I.T. Vargas, D.A. Fischer, M.A. Alsina, J.P. Pavissich, P.A. Pasten, G.E. Pizzaro, Copper corrosion and biocorrosion events in premise plumbing, Materials 10 (2017) 1–30, <https://doi.org/10.3390/ma10091036>
- [5] S. Neupane, P. Losada-Perez, U. Tiringner, P. Taheri, D. Desta, C. Xie, D. Cespo, A. Mol, I. Milosev, A. Kokalj, F.U. Renner, Study of mercaptobenzimidazoles as inhibitors for copper corrosion: down to the molecular scale, J. Electrochem. Soc. 168 (2021) 125–133, <https://doi.org/10.1149/1945-7111/abf9c3>
- [6] B. Tan, B. Xiang, S. Zhang, Y. Qiang, L. Xu, S. Chen, J. He, Papaya leaves extract as a novel eco-friendly corrosion inhibitor for Cu in H₂SO₄ medium, J. Col. Interf. Sci. 582 (2021) 918–931, <https://doi.org/10.1016/j.jcis.2020.08.093>
- [7] M. Aslan, Y. Akaltun, M. T. Yetimc, T. Çayır, A. Çelik, The effect of wettability on corrosion resistance of oxide films produced by SILAR method on magnesium, aluminum and copper substrates, Surf. Coat. Technol. 292 (2016) 121–131, <https://doi.org/10.1016/j.surfcoat.2016.03.011>
- [8] A. Hojabri, F. Hajakbrai, N. Soltanpoor, M.S. Hedayati, Effect of silver thickness on structural, optical and morphological properties of nanocrystalline Ag/NiO thin films, J. Theo. Appl. Phys. 8 (2014) 15–22, <https://doi.org/10.1007/s40094-018-0275-2>
- [9] H. Wu, X. Zhang, X. He, M. Li, X. Huang, R. Hang, B. Tang, Wear and corrosion resistance of anti-bacterial Ti–Cu–N coatings on titanium implants, Appl. Surf. Sci. 317 (2014) 614–621, <https://doi.org/10.1016/j.apsusc.2014.08.163>
- [10] F. Fracassi, R. d'Agostino, F. Palumbo, E. Angelini, S. Grassini, F. Rosalbino, Application of plasma deposited organosilicon thin films for the corrosion protection of metals, Surf. Coat. Technol. 174 (2003) 107–111, [https://doi.org/10.1016/S0257-8972\(03\)00422-5](https://doi.org/10.1016/S0257-8972(03)00422-5)
- [11] N.W. Farro, L. Veleva, P. Aguilar, Copper marine corrosion: I. Corrosion rates in atmospheric and seawater environments of Peruvian Port, Open Corros. J. 2 (2009) 130–138, <https://doi.org/10.2174/1876503300902010130>
- [12] L. Núñez, E. Reguera, F. Corvo, E. González, C. Vázquez, Corrosion of copper in seawater and its aerosols in a tropical island, Corros. Sci. 47 (2005) 461–484, <https://doi.org/10.1016/j.corsci.2004.05.015>
- [13] G. Kear, B.D. Barker, F.F. Walsh, Electrochemical corrosion of unalloyed copper in chloride media—a critical review, Corros. Sci. 46 (2004) 109–135, [https://doi.org/10.1016/S0010-938X\(02\)00257-3](https://doi.org/10.1016/S0010-938X(02)00257-3)
- [14] L. Vrsalović, S. Gudić, M. Kliškić, E.E. Oguzie, L. Carev, Inhibition of copper corrosion in NaCl solution by caffeic acid, Int. J. Electrochem. Sci. 11 (2016) 459–474.
- [15] R.K. Ahmed, S. Zhang, Alchemilla Vulgaris extract as green inhibitor of copper corrosion in hydrochloric acid, Int. J. Electrochem. Sci. 14 (2019) 10657–10669, <https://doi.org/10.20964/2019.11.43>
- [16] Ž.Z. Tasić, M.B.P. Mihajlović, M.B. Radovanović, M.M. Antonijević, Electrochemical investigations of copper corrosion inhibition by azithromycin in 0.9 % NaCl, J. Molec. Liq. 265 (2018) 687–692, <https://doi.org/10.1016/j.molliq.2018.03.116>
- [17] E.M. Sherif, Su-Moon Park, Inhibition of copper corrosion in 3.0 % NaCl solution by N-phenyl-1, 4-phenylenediamine, J. Electrochem. Soc. 152 (2005) B428–B435, <https://doi.org/10.1149/1.2018254>
- [18] N. Benzbiria, S. Echih, M.E. Belghiti, A. Thoume, A. Elmakssoudi, A. Zarrouk, M. Zertoubi, M. Azzi, Novel synthesized benzodiazepine as efficient corrosion inhibitor for copper in 3.5 % NaCl solution, Mater. Today 37 (2020) 3932–3939, <https://doi.org/10.1016/j.matpr.2020.09.030>
- [19] H.S. Bahari, H. Savaloni, Surface analysis of Cu coated with ALD Al₂O₃ and its corrosion protection enhancement in NaCl solution: EIS and polarization, Mater. Res. Express 6 (2019) 55–62, <https://doi.org/10.1088/2053-1591/ab1abd>
- [20] J. Percy, P. Sefhra, M. Baraneedharan, T. Sivakumar, D. Thangadurai, K. Nehru, CuO/SiO₂ modified amine functionalized reduced graphene oxide with enhanced photocatalytic and electrochemical properties, SN Appl. Sci. 1 (2018) 24–32, <https://doi.org/10.1007/s42452-018-0074-z>
- [21] S. Ghosh, S. Kundu, M.K. Naskar, Mesoporous CuO nanostructures for low-temperature CO oxidation, Bull. Mater. Sci. 44 (2021) 189–194, <https://doi.org/10.1007/s12034-021-02000-0>

- 1007/s12034-021-02475-6
- [232] L.C. Chen, C.C. Chen, K.C. Liang, S.H. Chang, Z.L. Tseng, S.C. Yeh, C.T. Chen, C.G. Wu, Efficiently visible-light driven photoelectrocatalytic oxidation of As (III) at low positive biasing using Pt/TiO₂ nanotube electrode, *Nanoscale Res. Lett.* 11 (2016) 32–45, <https://doi.org/10.1186/s11671-016-1248-5>
- [23] H. Solache-Carranco, G. Juarez-Diaz, J. Martinez-Juarez, R. Peña-Sierra, Estudio de la cristalización de Cu₂O y su caracterización por difracción de rayos X, espectroscópica Raman y fotoluminiscencia, *Rev. Mex. Fís.* 55 (2009) 393–398.
- [24] L. Debbichi, M.C. Marco de Lucas, J.F. Pierson, P. Krüger, Vibrational properties of CuO and Cu₄O₃ from first-principles calculations, and Raman and infrared spectroscopy, *J. Phys. Chem. C* 116 (2012) 10232–10237, <https://doi.org/10.1021/jp303096m>
- [25] A.S. Zoofakar, R.A. Rani, A.J. Morfa, A.P. O'Mullane, K. Kalantar-zadeh, Nanostructured copper oxide semiconductors: a perspective on materials, synthesis methods and applications, *J. Mater. Chem. C* 2 (2014) 5247–5270, <https://doi.org/10.1039/c4tc00345d>
- [26] M.Ma. Iğorzata Lachowicz, A metallographic case study of formicary corrosion in heat exchanger copper tubes, *Eng. Fail. Anal.* 111 (2020) 104502, <https://doi.org/10.1016/j.engfailanal.2020.104502>
- [27] T. Tzevelekiou, A. Flampouri, A. Rikos, A. Vazdirvanidis, G. Pantazopoulos, D. Skarmoutsos, Hot corrosion failure in the first stage nozzle of a gas turbine engine, *Eng. Fail. Anal.* 33 (2013) 176–185, <https://doi.org/10.1016/j.engfailanal.2015.11.057>
- [28] K. Chandra, V. Kain, P.S. Shetty, R. Kishan, Failure analysis of copper tube used in a refrigerating plant, *Eng. Fail. Anal.* 37 (2014) 1–11, <https://doi.org/10.1016/j.engfailanal.2013.11.014>
- [29] E. García, J. Uruchurtu, J. Genescá, Effect of the sea water components in the pitting corrosion of copper, *J. Met.* 31 (1995) 307–315, <https://doi.org/10.3989/revmetalm.1995.v31.i5.946>
- [30] T. Wei, R. Zhang, H. Yang, H. Liu, S. Qiu, Y. Wang, P. Du, K. He, X. Hu, C. Dong, Microstructure, corrosion resistance and oxidation behavior of Cr-coatings on Zircaloy-4 prepared by vacuum arc plasma deposition, *Corros. Sci.* 158 (2019) 108077, <https://doi.org/10.1016/j.corsci.2019.06.029>
- [31] Ö. Bayrak, H.G. Asl, A. Ak, Reduction of residual stress in porous Ti6Al4V by in situ double scanning during laser additive manufacturing, *Int. J. Min. Metall. Mater.* 27 (2020) 1269–1282, <https://doi.org/10.1007/s12613-020-2212-z>
- [32] V.V. Poplavsky, A.V. Dorozhko, V.G. Matys, Formation of catalytic and corrosion protective layers with use of ion beam assisted deposition of metals from vacuum arc discharge plasma, *J. Phys.* 2064 (2021) 012054, <https://doi.org/10.1088/1742-6596/2064/1/012054>
- [33] M.B. Valcarce, S.R. de Sánchez, M. Vázquez, Localized attack of copper and brass in tap water: the effect of Pseudomonas, *Corros. Sci.* 47 (2005) 795–809, <https://doi.org/10.1016/j.corsci.2004.07.013>
- [34] Y. Van Ingelgem, A. Hubin, J. Vereecken, Investigation of the first stages of the localized corrosion of pure copper combining EIS, FE-SEM and FE-AES, *Electrochim. Acta* 52 (2007) 7642–7650, <https://doi.org/10.1016/j.electacta.2006.12.039>
- [35] Q.Q. Liao, Z.W. Yue, D. Yang, Z.H. Wang, Z.H. Li, H.H. Ge, Y.J. Li, Inhibition of copper corrosion in sodium chloride solution by the self-assembled monolayer of sodium diethyldithiocarbamate, *Corros. Sci.* 53 (2011) 1999–2005, <https://doi.org/10.1016/j.corsci.2011.02.023>
- [36] K.F. Khaled, Studies of the corrosion inhibition of copper in sodium chloride solutions using chemical and electrochemical measurements, *Mater. Chem. Phys.* 125 (2011) 427–433, <https://doi.org/10.1016/j.matchemphys.2010.10.037>
- [37] H. Huang, Z. Wang, Y. Gong, F. Gao, Z. Luo, S. Zhang, H. Li, Water soluble corrosion inhibitors for copper in 3.5 wt % sodium chloride solution, *Corros. Sci.* 123 (2017) 339–350, <https://doi.org/10.1016/j.corsci.2017.05.009>